

1 **Replay to the review of: “Time dependent, non-monotonic response of warm**
2 **convective cloud fields to changes in aerosol loading”**

3

4 Dear Dr. Ervens,

5 We would like first to thank you for agreeing to take our paper and to complete the
6 review process so fast, it is highly appreciated. We also appreciate the time and efforts
7 you have put in reading the revised manuscript and our previous responses to the
8 referee comments. Please find below a point by point answers to your comments.

9

10 1. 10: Change ‘properties’ to ‘loading’ as you do not explore effects of any other
11 aerosol properties (composition, size)

12 **Answer:** Thank you for this correction. It was changed: *"Large Eddy Simulations*
13 *(LES) with bin microphysics are used here to study cloud fields’ sensitivity to changes*
14 *in aerosol loading and the time evolution of this response."*

15

16 2. 191: If the aerosol size distribution is only scaled up/down, the shape should be
17 identical, not similar

18 **Answer:** Thank you. Indeed the aerosol size distribution is constant. We have
19 corrected it in the revised manuscript: *"To reduce the results sensitivity to the shape of*
20 *the aerosol size distribution and to focus on the aerosol number concentration effect,*
21 *the different aerosol concentrations are calculated by multiplication of all bins by a*
22 *constant factor and maintaining a constant shape of the size distribution."*

23

24 3. 341: How does the study by Dagan et al., 2016, differ from the current one?

25 **Answer:** In Dagan et al. (2016) we did not discuss the aerosol effect on the mean
26 cloud field properties and their non-monotonic trend but only the thermodynamic
27 evolution. Changes in the thermodynamic conditions do change the cloud scale
28 processes and specifically the transition from cloud enhancement to suppression (i.e.
29 the evolution of the non-monotonic trend). Therefore this current paper is dedicated to
30 show the interplay between the evolution of the cloud field thermodynamic properties

31 and their interactions with the cloud scale non-monotonic behavior. Specifically, in
32 this study we examine the response of cloud fields' mean properties to changes in the
33 aerosol loading. This is done both globally (during the entire simulation period, Sec.
34 3.1) and for different periods along the simulation (Sec. 3.2). We show that the mean
35 field properties change in a non-monotonic trend, with an optimal aerosol
36 concentration that can be explained by contradicting aerosol effects on processes that
37 encourage cloud development versus those that suppress it. The time evolution of this
38 response and the increase in time of the optimal aerosol concentration are driven by
39 the evolution of the thermodynamic conditions that is different for different aerosol
40 loading conditions.

41 In line 341 we mentioned that the focus of Dagan et al. (2016) is the changes in the
42 thermodynamic evolution under different aerosol concentrations: "*All the aerosol*
43 *effects that were discussed up to this point (condensation-evaporation efficiencies, η*
44 *and water loading) are applicable both on the single cloud scale as well as on the*
45 *cloud field scale. However, on the cloud field scale, another aspect needs to be*
46 *considered, namely the time evolution of the effect of clouds on the field's*
47 *thermodynamic conditions (which was the focus of a recent study by Dagan et al.,*
48 *2016).*"

49

50 4. 374: either 'last' or 'third' seems redundant here

51 **Answer:** We have changed it in the revised manuscript: "*On the other hand, in the*
52 *more polluted simulations, (with aerosol loading of 250 and 500 cm^{-3}) there is an*
53 *increase in the total water mass with time (of 17 and 37% between the first and the*
54 *last periods of the simulations, respectively).*"

55

56 5. 381: a) There is no Figure 1F

57 b) I am confused (but this might be due to the missing figure): The rain rate is given
58 in mm/day (e.g. fig. 1F). How does this translate into percentages?

59 **Answer:** Thank you. Indeed this was a mistake. We corrected it in line 381 to "Fig.
60 6F". The revised manuscript: "*Trends in the mean rain rate show that in the cleanest*
61 *simulations (5, 25 and 50 cm^{-3}) it decreases with time (Fig. 6F, 53.3, 32.9 and 40.1%,*
62 *respectively). In the regime of medium to fairly high aerosol loading (100, 250 and*

63 500 cm^{-3}) the rain rate increases (19.6, 598.1 and 841.5%, respectively). And in the
64 most polluted simulations (2000 and 5000 cm^{-3}) the surface rain is negligible
65 throughout the simulation time. These trends are explained below."

66 As for all properties presented in Fig. 6 and table 1 we calculated the percentile
67 change between the last and first part of the simulation for better understanding its
68 time evolution. It is explained in the text: "Table 1 presents change (in percentage) in
69 the mean values of key variables between the third period of the 8 simulations (during
70 the 11:20-16:00 hours of simulation, red curves in Fig. 6) and the first period (02:00-
71 06:40 hours of simulation, blue curves in Fig. 6)".

72

73

74

75

76

77

78

79

80

81

82

83

84

85

86

87 **Time dependent, non-monotonic response of warm convective cloud fields to**
88 **changes in aerosol loading**

89 **Guy Dagan, Ilan Koren*, Orit Altaratz and Reuven H. Heiblum**

90 Department of Earth and Planetary Sciences, The Weizmann Institute of Science,
91 Rehovot 76100, Israel.

92 * *Correspondence to:* ilan.koren@weizmann.ac.il

93

94 **Abstract**

95 Large Eddy Simulations (LES) with bin microphysics are used here to study cloud
96 fields' sensitivity to changes in aerosol [properties-loading](#) and the time evolution of
97 this response. Similarly to the known response of a single cloud, we show that the
98 mean field properties change in a non-monotonic trend, with an optimum aerosol
99 concentration for which the field reaches its maximal water mass or rain yield. This
100 trend is a result of competition between processes that encourage cloud development
101 versus those that suppress it. However, another layer of complexity is added when
102 considering clouds' impact on the field's thermodynamic properties and how this is
103 dependent on aerosol loading. Under polluted conditions rain is suppressed and the
104 non-precipitating clouds act to increase atmospheric instability. This results in
105 warming of the lower part of the cloudy layer (in which there is net condensation) and
106 cooling of the upper part (net evaporation). Evaporation at the upper part of the
107 cloudy layer in the polluted simulations raises humidity at these levels and thus
108 amplifies the development of the next generation of clouds (preconditioning effect).
109 On the other hand, under clean conditions, the precipitating clouds drive net warming
110 of the cloudy layer and net cooling of the sub-cloud layer due to rain evaporation.
111 These two effects act to stabilize the atmospheric boundary layer with time
112 (consumption of the instability). Evolution of the field's thermodynamic properties
113 affects the cloud properties in return, as shown by migration of the optimal aerosol
114 concentration toward higher values.

115

116 **1. Introduction**

117 Despite the extensive research conducted in the last few decades, and the fact that
118 clouds have an important role in the Earth's energy balance (Trenberth et al., 2009)
119 clouds are still considered to be one of the largest source of uncertainty in the study of
120 climate and climate change (Forster et al., 2007; Boucher et al., 2013).

121 Warm cloud (containing liquid water only) formation depends on the availability of
122 water vapor and aerosols acting as cloud condensation nuclei (CCN). Changes in
123 aerosol concentration modulate the cloud droplet size distribution and total number.
124 Polluted clouds (forming under high aerosol loading) initially have smaller and more
125 numerous droplets, with narrower size distribution compared to clean clouds (Squires,
126 1958; Squires and Twomey, 1960; Warner and Twomey, 1967; Fitzgerald and Spyers-
127 Duran, 1973).

128 The initial droplet size distribution affects key cloud processes such as condensation-
129 evaporation, collision-coalescence and sedimentation. The condensation-evaporation
130 process is proportional to the total droplet surface area which increases with the
131 droplet number concentration (for a given total liquid water mass). Under given
132 supersaturation conditions, the condensation in polluted clouds is more efficient
133 (higher condensation rate or shorter consumption time of the supersaturation - Pinsky
134 et al., 2013; Seiki and Nakajima, 2014; Koren et al., 2014; Kogan and Martin, 1994;
135 Dagan et al., 2015a). However, under sub-saturation conditions, due to the same
136 reason, it implies higher evaporation efficiency. The evaporation induces downdrafts
137 and stronger vorticity and hence can lead to stronger mixing of the cloud with its
138 environment in polluted conditions (Xue and Feingold, 2006; Jiang et al., 2006; Small
139 et al., 2009).

140 The initiation of collision-coalescence is delayed in polluted clouds (Gunn and
141 Phillips, 1957; Squires, 1958; Albrecht, 1989). This drives a delay in rain formation
142 and can affect the amount of surface rain (Rosenfeld, 1999, 2000; Cheng et al., 2007;
143 Khain, 2009; Levin and Cotton, 2009; Koren et al., 2012; Hazra et al., 2013a,b; Dagan
144 et al., 2015b).

145 Aerosol effects on single warm convective clouds were shown to have an optimal
146 value with respect to maximal water mass, cloud depth and rain yield (Dagan et al.,

147 2015a,b), which depends on the environmental conditions. For aerosol concentrations
148 lower than the optimum, the positive relationship between aerosol concentration and
149 cloud development is a result of two main processes: 1) larger latent heat release
150 driven by the increase in the condensation efficiency causing stronger updrafts, and 2)
151 decrease in the effective terminal velocity (η , i.e. mass weighted terminal velocity of
152 the hydrometeors) (Koren et al., 2015) due to initial smaller droplets and the delay in
153 the collision-coalescence process. The smaller droplets have higher mobility (the
154 water mass moves up better with surrounding updraft), reaching higher in the
155 atmosphere and prolonging the cloud growth.

156 For aerosol concentration values above the optimum, the suppressing aerosol effects
157 take over, namely: 1) stronger mixing of the cloud with its environment driven by the
158 increased evaporation efficiency (Small et al., 2009), and 2) increased water loading
159 effect due to the rain suppression.

160 Understanding of the overall aerosol effect is even more complex when considering
161 processes on the cloud field scale. Clouds affect the surrounding thermodynamic
162 conditions by changing the humidity and temperature profiles (Lee et al., 2014;
163 Seifert et al., 2015; Stevens and Feingold, 2009; Saleeby et al., 2015). In addition,
164 clouds affect the solar and longwave radiation budgets in the field. Over land the
165 radiation effects change the surface temperature and therefore can significantly affect
166 heat and moist fluxes, and as a result the cloud properties (Koren et al., 2004, 2008;
167 Feingold et al., 2005).

168 The invigoration mechanism, which refers to deeper and larger clouds with larger
169 mass that develop under polluted conditions was studied mainly in deep convective
170 clouds (Andreae et al., 2004; Koren et al., 2005; Rosenfeld et al., 2008; Tao et al.,
171 2012; Fan et al., 2013; Hazra et al., 2013a; Altaratz et al., 2014). Our focus here is on
172 warm cloud fields for which previous observational studies reported on invigoration
173 effect or a non-monotonic response of the clouds to an increase in aerosol loading.
174 For example, Kaufman et al., (2005) found an increase in cloud fraction (CF) of warm
175 cloud fields with increasing aerosol loading over the tropical Atlantic Ocean. Yuan et
176 al. (2011) reported that an increase in volcanic aerosols near Hawaii led to increased
177 trade cumulus CF and clouds top height. Dey et al. (2011) have shown that an
178 increase in aerosol optical depth (AOD) from clean to slightly polluted resulted in an

179 increase in CF in warm clouds over the Indian Ocean. Additional increase in the AOD
180 resulted in a decrease of CF, explained by the semi direct effect of absorbing aerosols.
181 Costantino and Bréon (2013) reported higher CF over the south-eastern Atlantic under
182 high aerosol loading conditions. From convective stability considerations deeper
183 clouds tend to have larger area (larger CF). It was shown that warm convective
184 cloud's area correlates positively with cloud's depth (Benner and Curry, 1998; Koren
185 et al., 2008).

186

187 Koren et al. (2014) have shown that warm convective clouds over the Southern
188 Oceans can be considered as aerosol limited up to moderate aerosol loading
189 conditions. As the AOD increases, the clouds were shown to be deeper and larger, and
190 to produce stronger rain rates. A reversal in trend of liquid water path (LWP) as a
191 function of increasing AOD was reported using observations of warm convective
192 clouds under large range of meteorological conditions (Savane et al., 2015). Li et al.
193 (2011) studied warm clouds over the southern great plains of the United States and
194 reported no aerosol effect on clouds' top height.

195 On the other hand, numerical studies of the aerosol's effect on warm cumulus cloud
196 fields show either no effect or cloud suppression (meaning shallower and smaller
197 clouds under higher aerosol loading conditions). Jiang and Feingold (2006) found that
198 the LWP, CF, and cloud depth of warm shallow convective clouds are insensitive to
199 an increase in aerosol loading. However, they did demonstrate rain suppression by
200 aerosols. Xue et al. (2008) showed smaller clouds and suppression of precipitation in
201 increased aerosol loading environment. Jiang et al. (2010) found a non-monotonic
202 change in the derivative of the surface rain rate with aerosol loading (susceptibility)
203 for higher maximal LWP clouds, but a monotonic decrease in the total precipitation
204 with aerosol loading. Seigel (2014) showed that the clouds' size decreases with
205 aerosol loading due to enhanced entrainment at clouds' margins.

206 Some previous studies have demonstrated clouds alteration of their environment
207 (Zhao and Austin, 2005; Heus and Jonker, 2008; Malkus, 1954; Lee et al., 2014;
208 Zuidema et al., 2012; Roesner et al., 1990). One example of such effect is the
209 "preconditioning" or "cloud deepening" effect (Nitta and Esbensen, 1974; Roesner et
210 al., 1990; Stevens, 2007; Stevens and Seifert, 2008), where clouds cool and moisten

211 the upper cloudy and inversion layers and by that encourage the development of the
212 next generation of clouds that encounter improved environmental conditions. This
213 effect is influenced by the clouds' microphysical properties (Stevens and Feingold,
214 2009; Saleeby et al., 2015). The role of warm convective clouds in moistening of the
215 free troposphere was studied intensively using both observations and cloud field
216 numerical models (Brown and Zhang, 1997; Johnson et al., 1999; Takemi et al., 2004;
217 Kuang and Bretherton, 2006; Holloway and Neelin, 2009; Waite and Khouider,
218 2010).

219 Albrecht (1993) used a theoretical single column model to study the effect of
220 precipitation on the thermodynamic structure of trade wind boundary layer and found
221 that even low rain rates can dramatically affect the profiles. Under precipitating
222 conditions, the cloud layer is warmer, drier, and more stable than under non-
223 precipitation conditions. He also showed that under non-precipitating conditions the
224 inversion height is greater than under precipitating conditions, due to the larger
225 amount of liquid water evaporated at those elevations.

226 Another way clouds effect their environment is by evaporation of rain below the cloud
227 base which induces cooling of the sub-cloudy layer (Zuidema et al., 2012; Heiblum et
228 al., 2016a). Lee et al. (2014) demonstrated the aerosol effects on the field's CAPE (as
229 distributed above cloud base or below it). The organization of the field is influenced
230 by cloud processes as well. Enhanced evaporative cooling in the sub-cloud layer, for
231 example, can produce cold pools which enhance the generation of clouds only at their
232 boundaries, and hence change the organization of the field (Seigel, 2014; Seifert and
233 Heus, 2013; Heiblum et al., 2016a).

234 A recent paper (Dagan et al., 2016) showed that polluted clouds act to increase the
235 thermodynamic instability with time, while clean clouds consume the atmospheric
236 instability. The trend of the pollution driven increase in the instability is halted once
237 the clouds are thick enough to develop significant precipitation. Indeed, studies of
238 long simulation times (>30 hr), showed that the initial differences between clean and
239 polluted cases are reduced by negative feedbacks of the clouds on the thermodynamic
240 conditions (Lee et al., 2012; Seifert et al., 2015).

241 In this work we explore the coupled microphysical-dynamic system of warm marine
242 cloud fields using a bin-microphysics scheme under a large range of aerosol
243 concentrations. We study the aerosol-cloud-environmental thermodynamic system by
244 examining how changes in aerosol concentrations affect clouds properties, the related
245 modifications of the thermodynamic conditions over time which as well drive
246 feedbacks on the clouds' properties evolution.

247

248 **2. Methodology**

249 The SAM (System for Atmospheric Modeling), non-hydrostatic, anelastic LES model
250 version 6.10.3 (Khairoutdinov and Randall, 2003) was used to simulate the well-
251 studied trade cumulus case of BOMEX (Holland and Rasmusson, 1973; Siebesma et
252 al., 2003). The BOMEX case is an idealized trade-cumulus cloud field that is based on
253 observations made near Barbados during June 1969. This case was initialized using
254 the setup specified in Siebesma et al. (2003). The setup includes surface fluxes and
255 large scale forcing (see details in Heiblum et al., 2016b). The horizontal resolution
256 was set to 100 m while the vertical resolution was set to 40 m. The domain size was
257 $12.8 \times 12.8 \times 4.0 \text{ km}^3$ and the time step was 1 sec. Due to computational limitations,
258 we had to restrict the domain size to a scale that has a limited capability for capturing
259 large scale organization (Seifert and Heus, 2013). The model ran for sixteen hours and
260 the statistical analysis included all but the first two hours (total of 14 hours). After 2 h
261 of simulations the initial increase in the total liquid water mass in the domain desisted
262 and the differences between the simulations (differ by the aerosol loading) became
263 significant. Therefore 2h is determined as spin-up time (similar to the spin-up time in
264 Xue and Feingold, 2006).

265 A bin microphysical scheme (Khain and Pokrovsky, 2004) was used. The scheme
266 solves warm microphysical processes, including droplet nucleation, diffusional
267 growth, collision coalescence, sedimentation and breakup.

268 In order to focus on the aerosol effect on the thermodynamic properties of the field,
269 the radiative effects (as included in the large scale forcing - see details in Dagan et al.,
270 2016) were prescribed in all simulations. The aerosol distribution adopts a marine size
271 distribution (see details in Jaenicke 1988 and Altaratz et al., 2008). Eight different
272 simulations were conducted simulating a wide range of aerosol loading conditions
273 from extremely pristine to polluted (total concentration of: 5, 25, 50, 100, 250, 500,
274 2000 and 5000 cm^{-3} near ground level, Dagan et al., 2015a). To reduce the results

275 sensitivity to the shape of the aerosol size distribution and to focus on the aerosol
276 number concentration effect, the different aerosol concentrations are calculated by
277 multiplication of all bins by a constant factor and maintaining a similar-constant shape
278 of the size distribution. The aerosol is assumed to be composed of ammonium-sulfate
279 and initialized with constant mixing ratio with height. A prognostic equation is solved
280 for the aerosol mass, including regeneration upon evaporation and removal by surface
281 rain. Regeneration upon evaporation of cloud drops was shown to be a very important
282 source of aerosols, especially in polluted conditions (Yin et al., 2005). The aerosol
283 serves as potential cloud condensation nuclei (CCN) and it is activated based on the
284 Kohler theory (the scheme is described in Khain et al., 2000). The aerosol (water
285 drop) size distribution is calculated between 5 nm to 2 μm (2 μm -3.2 μm). For both
286 aerosol and drops, successive bins represent doubling of the mass.
287 The effects of changes in aerosol concentration on the drop concentration and its
288 mean size, for the different simulations can be found in Fig. S1 in the supporting
289 information (SI).

290

291 **3. Results and discussion**

292 **3.1 Mean cloud field properties under different aerosol loading conditions**

293 The aerosol effects on the mean field properties during the entire run are examined
294 first following by a more detailed examination of the time evolution in the next
295 section. Figure 1 presents mean values of key properties of cloud fields as a function
296 of the aerosol loading for the entire (14 h) simulation time.

297 The total water mass (calculated as mean over time in each domain) as a function of
298 aerosol concentration shows a clear reversal in the trend (Fig. 1A). For the given
299 environmental conditions simulated here, it increases when increasing aerosol loading
300 from 5 to 50 cm^{-3} . Additional increase in the aerosol loading results in a decrease in
301 the total water mass in the domain.

302 The LWP (Liquid Water Path - Fig. 1B) calculated as a mean over time over all
303 cloudy columns in each domain, which is strongly correlated with the total water
304 mass, also shows the same non-monotonic general trend. The maximum in the curve
305 of cloudy LWP is at slightly higher aerosol concentration compared to the total mass
306 (100 cm^{-3}). This difference can be explained by the link to the cloud fraction (CF –
307 calculated as the area covered by clouds with optical path $\tau > 0.3$ Fig. 1C) that
308 decreases above aerosol loading of 25 cm^{-3} . And so, for the more polluted simulations

309 the mass is distributed on smaller horizontal cloud areas as shown in previous studies
310 (Seigel, 2014).

311

312 There is also a significant difference in the way the water mass is distributed along the
313 atmospheric column in the different simulations. The maximum cloud top height (Fig.
314 1D), calculated as a mean over time of the altitude of the highest grid box in the
315 domain that contains liquid water content ($LWC > 0.01 \text{ g/kg}$) increases significantly
316 when increasing aerosol loading up to 500 cm^{-3} (increase from 1692 m to 2120 m
317 when increasing aerosol loading from 5 to 500 cm^{-3}). Additional increase in the
318 aerosol loading results in a minor decrease in the maximum cloud top height (down to
319 2030 m for aerosol loading of 5000 cm^{-3}). The minor decrease seen for this range of
320 aerosol concentration (compared with the larger decrease in the mean LWP for
321 example) can be explained by the location of the maximal cloud top height above the
322 cloud core, which is affected mainly by the invigoration processes (enhanced
323 condensation and latent heat release) and less by margin oriented processes (enhanced
324 entrainment and evaporation) that significantly impact the total cloud mass (Dagan et
325 al., 2015a). Another reason is the cloud deepening effect under polluted conditions
326 (Stevens, 2007; Seifert et al., 2015) that will be described later. As for the mean cloud
327 top height calculated as a mean of all cloudy columns along the whole run (Fig. 1E),
328 the trend shows a monotonic increase with aerosol loading. The trend is approaching a
329 saturation level for high aerosol concentration values. The mean cloud top value over
330 the simulation is 810 and 1010 m for the simulations with aerosol loading of 5 to 5000
331 cm^{-3} , respectively.

332 Presenting together the mean over time of the maximum and the mean cloud top
333 height captures, in a compact, yet informative, way the response of the cloud top
334 height distribution to changes in aerosol loading and reduces the sensitivity to outliers.
335 Moreover, by averaging over time the significance of the outliers is decreased as well.

336

337 The trend in the domain's average rain rate, as a function of the aerosol loading (Fig.
338 1F) shows a peak at relatively low aerosol loading (similar to optimal value of the CF)
339 of 25 cm^{-3} .

340

341 Fig. 2 presents the vertical profiles of the total condensed and evaporated mass during
342 the simulations, for four different simulations. We note that as the aerosol loading
343 increases, both the condensed and evaporated mass increased (this is due to the
344 increase in the diffusion rates – see Fig. S2, SI, and despite the decrease in cloud
345 fraction – see Fig. 1C, Dagan et al., 2015a; Koren et al., 2014; Pinsky et al., 2013;
346 Seiki and Nakajima, 2014). Below cloud base (located around 550 m) the clean
347 simulations have small rain evaporation values which is absent in the polluted
348 simulations.

349

350 Effective terminal velocity (η) is defined as the mass weighted average terminal
351 velocity of all the hydrometeors within a given volume of air (Koren et al., 2015). By
352 definition, η measures the terminal velocity of the water mass's center of gravity
353 (COG), i.e. the COG's movement with respect to the surrounding air's vertical
354 velocity (W). Small absolute values $|\eta|$ imply that the droplets COG will move better
355 with the surrounding air, i.e. the droplets will have better mobility (Koren et al.,
356 2015). The sum $V_{COG} = W + \eta$ (η always negative) reflects the water mass COG
357 vertical velocity relative to the surface. Positive V_{COG} implies a rise of the COG, and
358 negative value means falling.

359 The mean updraft (in both space and time, weighted by the liquid water mass in each
360 grid box to be consistent with the COG point of view - Fig. 3A) increases with the
361 increase in aerosol loading, in agreement with previous studies (Saleeby et al., 2015;
362 Seigel, 2014). This indicates an increase in the latent heat contribution to the cloud
363 buoyancy, driven by increase in the condensation efficiency (Dagan et al., 2015a,b;
364 Koren et al., 2014; Pinsky et al., 2013; Seiki and Nakajima, 2014) (Fig. 2 and Fig S2,
365 SI). At the same time, $|\eta|$ decreases as the aerosol concentration increases (Fig. 3B)
366 indicating better mobility of the smaller droplets, allowing them to move more easily
367 with the air's updrafts. The outcome of these two effects is an increased V_{COG} for
368 higher aerosol concentration (Fig. 3C) indicating that the polluted clouds' liquid water
369 is pushed higher in the atmosphere (Koren et al., 2015) as shown by higher COG (Fig.
370 3D).

371

372 The mean COG height of the water mass (Grabowski et al., 2006; Koren et al., 2009)
373 (Fig. 3D), increases with the aerosol loading up to a relatively high concentration (500
374 cm^{-3}). Note that while the trend in the system's characteristic velocities (η and W) is
375 monotonic increase, the COG has an optimal aerosol concentration for which it
376 reaches its maximum height (500 cm^{-3}). For aerosol concentrations above 500 cm^{-3} a
377 minor decrease is shown. As described above, the COG height increase with aerosol
378 loading, between extremely clean and polluted conditions, can be explained by
379 increased V_{COG} , which is a product of both lower $|\eta|$ and increased updraft in the
380 cloud scale, and larger thermodynamic instability induced by the polluted clouds in
381 the field scale as will be shown in the next section (Dagan et al., 2016; Heiblum et al.,
382 2016a). The reduction of the mean COG height in the most polluted simulations is
383 caused by cloud suppressing processes including an enhanced entrainment (see the
384 enhanced evaporation efficiency with aerosol loading – Fig. 2 and Fig. S2, SI) and
385 larger water loading (Dagan et al., 2015a - shown also in Fig. 4a below).
386 The trend in COG height can be also viewed (in more detail) in Fig. 4a that presents
387 profiles of mean LWC for cloudy voxels only.

388 We show that both the height and the magnitude of the maximum LWC increase with
389 the aerosol loading. This is due to both rain suppression (Fig. 1F) and an increased
390 V_{COG} (Fig. 3C) with aerosol loading. There is a reduction in the mean LWP (for >100
391 cm^{-3} - Fig. 1B) although there is an increase in the LWC with aerosol loading due to
392 the differences in cloud fraction (Fig. 1C) and in the vertical distribution of the liquid
393 water (Fig. 4b). At the upper part of the clouds ($H>2000\text{m}$), in the polluted case, a
394 small amount of cloudy pixels have a large mean LWC (and hence a large water
395 loading effect) but the total amount of liquid water is small (Fig. 4b). Below the
396 clouds' base ($H\sim 550\text{m}$) the LWC trend is reversed due to the enhancement of rain in
397 the clean runs (Fig. 1F). The increase in LWC with aerosol loading implies a larger
398 water loading negative component in the clouds' buoyancy.

399

400 All the evidence presented in Figs. 2-4 explains the non-monotonic trends of the
401 clouds properties response to changes in aerosol loading (Fig. 1). For clean conditions
402 (below the optimal aerosol concentration value), an increase in aerosol loading would
403 enhance the cloud development (larger mass, LWP, cloud top, CF, rain rate) because

404 of two main factors: 1) an increase in the condensation efficiency (due to the larger
405 total droplet surface area for condensation and longer time- Fig. 2 and Fig S2, SI), and
406 2) smaller effective terminal velocity (η) values, that per given updraft allow the
407 cloud's hydrometeors to be pushed higher in the atmosphere (Koren et al., 2015) (Fig.
408 3B).

409 The higher condensation efficiency in polluted clouds (Fig. 2) results in a larger latent
410 heat release that enhances the updraft (Fig. 3A) and cloud development. The increased
411 V_{COG} reflects the two cloud enhancing processes (decrease in $|\eta|$ and larger mean
412 updraft). We note that the increase in the mean updraft values with aerosol loading is
413 seen despite the negative effect of water loading (see Fig. 4a). For aerosol
414 concentrations above the optimum, cloud development is suppressed by the increase
415 in evaporation efficiency (Fig. 2) and hence stronger mixing of the cloud with its
416 environment (i.e. Small et al., 2009), and larger water loading due to rain suppression
417 (Dagan et al., 2015a, Fig. 4a).

418

419

420

421 **3.2 The time evolution of the mean cloud field properties under different aerosol** 422 **loading conditions**

423 All the aerosol effects that were discussed up to this point (condensation-evaporation
424 efficiencies, η and water loading) are applicable both on the single cloud scale as well
425 as on the cloud field scale. However, on the cloud field scale, another aspect needs to
426 be considered, namely the time evolution of the effect of clouds on the field's
427 thermodynamic conditions (which was the focus of a recent study by Dagan et al.,
428 2016).

429 Figure 5 presents the changes (final value minus initial one) in the temperature (T)
430 and water vapor content (q_v) vertical profiles as a function of aerosol concentration
431 used in the simulation. The initial profiles were identical in all simulations. Figure S3
432 (in the SI) presents the full temporal evolution of those parameters. In low aerosol
433 concentration runs (100 cm^{-3} and below) the sub-cloud layer becomes cooler and
434 wetter with time and the cloudy layer warmer and drier. Meanwhile, under higher

435 aerosol concentrations conditions (250 cm^{-3} and above) the sub-cloud layer becomes
436 warmer and drier while the cloudy and inversion layers become colder and wetter.
437 This trend is driven by the condensation-evaporation tendencies along the vertical
438 profile (see Fig. 2, Dagan et al., 2016). Under low aerosol concentration conditions,
439 water condenses at the cloudy layer and is advected downward to the sub-cloud layer
440 where it partially evaporates. Under polluted conditions, on the other hand, the
441 condensed water from the lower part of the cloudy layer is advected up to the upper
442 cloudy and inversion layers (driven by larger V_{COG} - Fig. 3) and evaporates there
443 (Dagan et al., 2016).

444

445 Such trends in the environmental thermodynamic conditions are likely to affect the
446 forming clouds. In Fig. 6 the time evolution of some of the key cloud field properties
447 are considered (the same properties that were shown in Fig. 1). The blue, green and
448 red curves represent the mean values over the first, second and third periods of the
449 simulations, respectively (each one covers 4 hours and 40 min). Table 1 presents
450 change (in percentage) in the mean values of key variables between the third period of
451 the 8 simulations (during the 11:20-16:00 hours of simulation, red curves in Fig. 6)
452 and the first period (02:00-06:40 hours of simulation, blue curves in Fig. 6).

453 Examination of the evolution in the mean total water mass along the simulations (Fig.
454 6A blue, green and red curves) presents a different trend between the clean and the
455 polluted simulations. In the clean simulations ($5\text{-}100 \text{ cm}^{-3}$) the total water mass
456 decreases significantly with time (a decrease of 57, 45, 44, 20% in the total mass for
457 the cases of 5, 25, 50 and 100 cm^{-3} respectively – see table 1). On the other hand, in
458 the more polluted simulations, (with aerosol loading of 250 and 500 cm^{-3}) there is an
459 increase in the total water mass with time (of 17 and 37% between the first and the
460 last ~~third~~ periods of the simulations, respectively). Under extreme polluted conditions
461 of 2000 and 5000 cm^{-3} , the total water mass in the domain is small and there is little
462 change with time. These changes in time push the optimum aerosol concentration to
463 higher values along the simulation time. This trend is also shown for the optimum
464 aerosol concentration with regard to the mean cloudy LWP (Fig. 6B), max top (Fig.
465 6D) and mean top (Fig. 6E).

466 Trends in the mean rain rate show that in the cleanest simulations (5, 25 and 50 cm⁻³)
467 it decreases with time (Fig. 4H6F, 53.3, 32.9 and 40.1%, respectively). In the regime
468 of medium to fairly high aerosol loading (100, 250 and 500 cm⁻³) the rain rate
469 increases (19.6, 598.1 and 841.5%, respectively). And in the most polluted
470 simulations (2000 and 5000 cm⁻³) the surface rain is negligible throughout the
471 simulation time. These trends are explained below.

472

473 The time evolution of the thermodynamic conditions (Fig. 5) shows a reduction
474 (enhancement) in the thermodynamic instability with time in the clean (polluted)
475 simulations. Figure 6 and table 1 indicate that under clean conditions the decrease in
476 the thermodynamic instability with time leads to a decrease in the mean cloud field
477 properties such as total mass, cloud top height and rain rate. Under polluted conditions
478 the trends are opposite and the mean cloud field properties increase with time due to
479 the increase in thermodynamic instability (Dagan et al., 2016) and due to the cloud
480 deepening (Stevens and Seifert, 2008; Stevens, 2007; Seifert et al., 2015). These
481 differences between the clean and polluted simulations drive changes in the optimum
482 aerosol concentration with time. For example, for the LWP (Fig. 1B) the optimum
483 aerosol concentration is 50, 100 and 250 cm⁻³ for the first, second and third parts of
484 the simulation, respectively.

485

486 **Summary**

487 Cloud processes can be divided in a simplistic manner into two characteristic scales –
488 the cloud scale and the field scale. Here using LES model with bin microphysical
489 scheme we studied the outcome of the two scales' processes acting together. We first
490 presented domain averaged properties over the whole simulation time (section 3.1) to
491 indicate the general aerosol effects in a first order manner and then we followed the
492 time evolution of the effects (section 3.2).

493 A non-monotonic aerosol effect was reported recently for a single cloud scale (Dagan
494 et al., 2015a,b). Here we show that these trends “survived” the domain and time
495 averaging. We argue that the enhanced development branch trend is driven by two
496 main processes of enhanced condensation and reduced effective terminal velocity
497 (which improves the droplets mobility). These processes are mainly related to the core

498 of the clouds and to the early stages of clouds development. We show that the cloud's
499 systems characteristic velocities can capture these effects. The effective terminal
500 velocity (η) inversely measures the mobility. Smaller droplets with smaller variance
501 will have smaller η and therefore will be pushed higher in a given updraft, whereas
502 larger droplets with larger η will deviate downward faster from the surrounding air.
503 Increase in condensation efficiency drives more latent heat release that enhances the
504 cloud updraft. We showed that V_{COG} is a product of the two velocities.

505 The descending branch in which increase of aerosol loading suppresses cloud
506 development is governed by increase in the evaporation efficiency on the subsaturated
507 parts of the clouds and by increase in water loading.

508 Since clouds change the atmospheric thermodynamic conditions in which they form,
509 different initial clouds would cause different impact on the environment. Therefore,
510 cloud field is a continuously evolving system for which aerosol properties determine
511 an important part of the temporal trends. Figure 5 shows striking differences between
512 the evolution of the thermodynamic profiles in clean and polluted cases. For the
513 polluted clouds (mostly non-precipitating), the upper cloudy layer turns wetter and
514 cooler due to enhanced evaporation and the sub-cloudy layer becomes warmer and
515 drier, which altogether act to increase the instability. On the other hand, clean
516 precipitating clouds consume the initial instability with time by warming the cloudy
517 layer (due to latent heat release) and cooling the sub-cloud layer by evaporation of
518 rain.

519 The polluted cloud feedbacks on the thermodynamic conditions act to deepen the
520 clouds. Since clouds that form in a more unstable environment are expected to be
521 aerosol limited up to higher aerosol concentrations (Koren et al., 2014; Dagan et al.,
522 2015a), an increase in the domains instability for the polluted cases drives an increase
523 in the optimal aerosol concentration with time.

524 We note that such an increase in the instability cannot last forever. A deepened cloud
525 will eventually produce larger precipitation rates that may weaken the overall effect
526 on the field (Stevens and Feingold, 2009; Seifert et al., 2015). These results pose an
527 interesting question on the dynamical state of cloud fields in nature. Do the cloud
528 fields 'manage' to reach a "near-equilibrium" state (Seifert et al., 2015), for which the
529 deepening effect balances the aerosol effect fast enough that the effects are buffered
530 most of the time (Stevens and Feingold, 2009). Or maybe, the characteristic lifetime

531 of a trade cumulus cloud field is shorter than the time it takes to significantly balance
532 the aerosol effects. In this case the cloud fields could be regarded as ‘transient’ and
533 therefore, as shown here, aerosol might have a strong effect on the clouds, both
534 through affecting the microphysics, initiating many feedbacks in the cloud scale, and
535 by affecting the field thermodynamic evolution over time.

536

537 **Acknowledgements**

538 This research has been supported by the Minerva foundation with funding from the
539 Federal German Ministry of Education and Research.

540

541 **References**

- 542 Albrecht, B. A.: Aerosols, cloud microphysics, and fractional cloudiness, *Science* (New York,
543 NY), 245, 1227, 1989.
- 544 Albrecht, B. A.: Effects of precipitation on the thermodynamic structure of the trade wind
545 boundary layer, *Journal of Geophysical Research: Atmospheres* (1984–2012), 98,
546 7327-7337, 1993.
- 547 Altaratz, O., Koren, I., Reisin, T., Kostinski, A., Feingold, G., Levin, Z., and Yin, Y.:
548 Aerosols' influence on the interplay between condensation, evaporation and rain in
549 warm cumulus cloud, *Atmospheric Chemistry and Physics*, 8, 15-24, 2008.
- 550 Altaratz, O., Koren, I., Remer, L., and Hirsch, E.: Review: Cloud invigoration by aerosols—
551 Coupling between microphysics and dynamics, *Atmospheric Research*, 140, 38-60,
552 2014.
- 553 Andreae, M. O., Rosenfeld, D., Artaxo, P., Costa, A. A., Frank, G. P., Longo, K. M., and
554 Silva-Dias, M. A. F.: Smoking rain clouds over the Amazon, *Science*, 303, 1337-
555 1342, 10.1126/science.1092779, 2004.
- 556 Benner, T. C., and J. A. Curry: Characteristics of small tropical cumulus clouds and their
557 impact on the environment, *J. Geophys. Res.*, 103(D22), 28753–28767,
558 doi:10.1029/98JD02579, 1998. Boucher, O., Randall, D., Artaxo, P., Bretherton, C.,
559 Feingold, G., Forster, P., Kerminen, V., Kondo, Y., Liao, H., and Lohmann, U.:
560 Clouds and aerosols, *Climate Change*, 571-657, 2013.
- 561 Brown, R. G., and Zhang, C.: Variability of midtropospheric moisture and its effect on cloud-
562 top height distribution during TOGA COARE*, *Journal of the atmospheric sciences*,
563 54, 2760-2774, 1997.
- 564 Cheng, C.-T., W.-C. Wang, and J.-P. Chen: A modelling study of aerosol impacts on cloud
565 microphysics and radiative properties, *Quarterly Journal of the Royal Meteorological*
566 *Society*, 133(623), 283-297, 2007.
- 567 Costantino, L., and Bréon, F.-M.: Aerosol indirect effect on warm clouds over South-East
568 Atlantic, from co-located MODIS and CALIPSO observations, *Atmospheric*
569 *Chemistry and Physics*, 13, 69-88, 2013.
- 570 Dagan, G., Koren, I., and Altaratz, O.: Competition between core and periphery-based
571 processes in warm convective clouds—from invigoration to suppression, *Atmospheric*
572 *Chemistry and Physics*, 15, 2749-2760, 2015a.
- 573 Dagan, G., Koren, I., and Altaratz, O.: Aerosol effects on the timing of warm rain processes,
574 *Geophysical Research Letters*, 42, 4590-4598, 10.1002/2015GL063839, 2015b.

575 Dagan, G., Koren, I., Altaratz, O., and Heiblum, R. H.: Aerosol effect on the evolution of the
576 thermodynamic properties of warm convective cloud fields, *Scientific Reports* **6**,
577 38769, 2016.

578 Dey, S., Di Girolamo, L., Zhao, G., Jones, A. L., and McFarquhar, G. M.: Satellite-observed
579 relationships between aerosol and trade-wind cumulus cloud properties over the
580 Indian Ocean, *Geophysical Research Letters*, **38**, 2011.

581 Fan, J., Leung, L. R., Rosenfeld, D., Chen, Q., Li, Z., Zhang, J., and Yan, H.: Microphysical
582 effects determine macrophysical response for aerosol impacts on deep convective
583 clouds, *Proceedings of the National Academy of Sciences*, **110**, E4581-E4590, 2013.

584 Feingold, G., Jiang, H. L., and Harrington, J. Y.: On smoke suppression of clouds in
585 Amazonia, *Geophysical Research Letters*, **32**, 10.1029/2004gl021369, 2005.

586 Fitzgerald, J., and Spyers-Duran, P.: Changes in cloud nucleus concentration and cloud
587 droplet size distribution associated with pollution from St. Louis, *Journal of Applied
588 Meteorology*, **12**, 511-516, 1973.

589 Forster, P., Ramaswamy, V., Artaxo, P., Berntsen, T., Betts, R., Fahey, D. W., Haywood, J.,
590 Lean, J., Lowe, D. C., Myhre, G., Nganga, J., Prinn, R., Raga, G., Schulz, M., and
591 Dorland, R. V.: Changes in Atmospheric Constituents and in Radiative Forcing., in:
592 *Climate Change 2007: The Physical Science Basis. Contribution of Working Group I
593 to the Fourth Assessment Report of the Intergovernmental Panel on Climate Change*,
594 edited by: Solomon, S., D. Qin, M. Manning, Z. Chen, M. Marquis, K.B. Averyt,
595 M.Tignor and H.L. Miller Cambridge University Press, Cambridge, United Kingdom
596 and New York, NY, USA., 2007.

597 Grabowski, W., Bechtold, P., Cheng, A., Forbes, R., Halliwell, C., Khairoutdinov, M., Lang,
598 S., Nasuno, T., Petch, J., and Tao, W. K.: Daytime convective development over land:
599 A model intercomparison based on LBA observations, *Quarterly Journal of the Royal
600 Meteorological Society*, **132**, 317-344, 2006.

601 Gunn, R., and Phillips, B.: An experimental investigation of the effect of air pollution on the
602 initiation of rain, *Journal of Meteorology*, **14**, 272-280, 1957.

603 Hazra, A., B. Goswami, and J.-P. Chen: Role of interactions between aerosol radiative effect,
604 dynamics, and cloud microphysics on transitions of monsoon intraseasonal
605 oscillations, *Journal of the Atmospheric Sciences*, **70**(7), 2073-2087, 2013a.

606 Hazra, A., P. Mukhopadhyay, S. Taraphdar, J. P. Chen, and W. R. Cotton: Impact of aerosols
607 on tropical cyclones: An investigation using convection-permitting model simulation,
608 *Journal of Geophysical Research: Atmospheres*, **118**(13), 7157-7168, 2013b.

609 Heiblum, R. H., Altaratz, O., Koren, I., Feingold, G., Kostinski, A. B., Khain, A. P.,
610 Ovchinnikov, M., Fredj, E., Dagan, G., and Pinto, L.: Characterization of cumulus
611 cloud fields using trajectories in the center-of-gravity vs. water mass phase space.
612 Part II: Aerosol effects on warm convective clouds, *Journal of Geophysical Research:
613 Atmospheres*, 2016a.

614 Heiblum, R. H., Altaratz, O., Koren, I., Feingold, G., Kostinski, A. B., Khain, A. P.,
615 Ovchinnikov, M., Fredj, E., Dagan, G., and Pinto, L.: Characterization of cumulus
616 cloud fields using trajectories in the center of gravity versus water mass phase space:
617 1. Cloud tracking and phase space description, *Journal of Geophysical Research:
618 Atmospheres*, 2016b.

619 Heus, T., and Jonker, H. J.: Subsiding shells around shallow cumulus clouds, *Journal of the
620 Atmospheric Sciences*, **65**, 1003-1018, 2008.

621 Holland, J. Z., and Rasmusson, E. M.: Measurements of the atmospheric mass, energy, and
622 momentum budgets over a 500-kilometer square of tropical ocean, *Monthly Weather
623 Review*, **101**, 44-55, 1973.

624 Holloway, C. E., and Neelin, J. D.: Moisture vertical structure, column water vapor, and
625 tropical deep convection, *Journal of the atmospheric sciences*, **66**, 1665-1683, 2009.

626 Jaenicke, R.: Aerosol physics and chemistry, *Landolt-Börnstein Neue Serie 4b*, 391-457,
627 1988.

628 Jiang, H., Xue, H., Teller, A., Feingold, G., and Levin, Z.: Aerosol effects on the lifetime of
629 shallow cumulus, *Geophysical Research Letters*, 33, 10.1029/2006gl026024, 2006.

630 Jiang, H., Feingold, G., and Sorooshian, A.: Effect of aerosol on the susceptibility and
631 efficiency of precipitation in warm trade cumulus clouds, *Journal of the Atmospheric*
632 *Sciences*, 67, 3525-3540, 2010.

633 Jiang, H. L., and Feingold, G.: Effect of aerosol on warm convective clouds: Aerosol-cloud-
634 surface flux feedbacks in a new coupled large eddy model, *Journal of Geophysical*
635 *Research-Atmospheres*, 111, D01202 10.1029/2005jd006138, 2006.

636 Johnson, R. H., Rickenbach, T. M., Rutledge, S. A., Ciesielski, P. E., and Schubert, W. H.:
637 Trimodal characteristics of tropical convection, *Journal of climate*, 12, 2397-2418,
638 1999.

639 Kaufman, Y. J., Koren, I., Remer, L. A., Rosenfeld, D., and Rudich, Y.: The effect of smoke,
640 dust, and pollution aerosol on shallow cloud development over the Atlantic Ocean,
641 *Proceedings of the National Academy of Sciences of the United States of America*,
642 102, 11207-11212, 10.1073/pnas.0505191102, 2005.

643 Khain, A. P., M. Ovchinnikov, M. Pinsky, A. Pokrovsky, and H. Krugliak: Notes on the state-
644 of-the-art numerical modeling of cloud microphysics, *Atmos. Res.*, 55(3-4), 159-
645 224, doi:10.1016/S0169-8095(00)00064-8, 2000.

646 Khain, A., and Pokrovsky, A.: Simulation of effects of atmospheric aerosols on deep turbulent
647 convective clouds using a spectral microphysics mixed-phase cumulus cloud model.
648 Part II: Sensitivity study, *Journal of the Atmospheric Sciences*, 61, 2983-3001,
649 10.1175/jas-3281.1, 2004.

650 Khain, A. P.: Notes on state-of-the-art investigations of aerosol effects on precipitation: a
651 critical review, *Environmental Research Letters*, 4, 015004 (015020 pp.)-015004
652 (015020 pp.), 10.1088/1748-9326/4/1/015004, 2009.

653 Khairoutdinov, M. F., and Randall, D. A.: Cloud resolving modeling of the ARM summer
654 1997 IOP: Model formulation, results, uncertainties, and sensitivities, *Journal of the*
655 *Atmospheric Sciences*, 60, 2003.

656 Kogan, Y. L., and Martin, W. J.: Parameterization of bulk condensation in numerical cloud
657 models, *Journal of the atmospheric sciences*, 51, 1728-1739, 1994.

658 Koren, I., Kaufman, Y. J., Remer, L. A., and Martins, J. V.: Measurement of the effect of
659 Amazon smoke on inhibition of cloud formation, *Science*, 303, 1342-1345,
660 10.1126/science.1089424, 2004.

661 Koren, I., Kaufman, Y. J., Rosenfeld, D., Remer, L. A., and Rudich, Y.: Aerosol invigoration
662 and restructuring of Atlantic convective clouds, *Geophysical Research Letters*, 32,
663 10.1029/2005gl023187, 2005.

664 Koren, I., Martins, J. V., Remer, L. A., and Afargan, H.: Smoke invigoration versus inhibition
665 of clouds over the Amazon, *Science*, 321, 946-949, 10.1126/science.1159185, 2008.

666 Koren, I., Oreopoulos, L., Feingold, G., Remer, L. A., and Altaratz, O.: How small is
667 a small cloud?, *Atmos. Chem. Phys.*, 8, 3855-3864, 2008.

668 Koren, I., Altaratz, O., Feingold, G., Levin, Z., and Reisin, T.: Cloud's Center of Gravity - a
669 compact approach to analyze convective cloud development, *Atmospheric Chemistry*
670 *and Physics*, 9, 155-161, 2009.

671 Koren, I., Altaratz, O., Remer, L. A., Feingold, G., Martins, J. V., and Heiblum, R. H.:
672 Aerosol-induced intensification of rain from the tropics to the mid-latitudes, *Nature*
673 *Geoscience*, 2012.

674 Koren, I., Dagan, G., and Altaratz, O.: From aerosol-limited to invigoration of warm
675 convective clouds, *science*, 344, 1143-1146, 2014.

676 Koren, I., Altaratz, O., and Dagan, G.: Aerosol effect on the mobility of cloud droplets,
677 *Environmental Research Letters*, 10, 104011, 2015.

678 Kuang, Z., and Bretherton, C. S.: A mass-flux scheme view of a high-resolution simulation of
679 a transition from shallow to deep cumulus convection, *Journal of the Atmospheric*
680 *Sciences*, 63, 1895-1909, 2006.

681 Lee, S.-S., Feingold, G., and Chuang, P. Y.: Effect of aerosol on cloud–environment
682 interactions in trade cumulus, *Journal of the Atmospheric Sciences*, 69, 3607-3632,
683 2012.

684 Lee, S. S., Kim, B.-G., Lee, C., Yum, S. S., and Posselt, D.: Effect of aerosol pollution on
685 clouds and its dependence on precipitation intensity, *Climate Dynamics*, 42, 557-577,
686 2014.

687 Levin, Z., and Cotton, W. R.: *Aerosol pollution impact on precipitation: A scientific review*,
688 Springer, 2009.

689 Li, Z., Niu, F., Fan, J., Liu, Y., Rosenfeld, D., and Ding, Y.: Long-term impacts of aerosols on
690 the vertical development of clouds and precipitation, *Nature Geoscience*, 4, 888-894,
691 10.1038/ngeo1313, 2011.

692 Nitta, T., and Esbensen, S.: Heat and moisture budget analyses using BOMEX data, *Monthly*
693 *Weather Review*, 102, 17-28, 1974.

694 Pinsky, M., Mazin, I., Korolev, A., and Khain, A.: Supersaturation and diffusional droplet
695 growth in liquid clouds, *Journal of the Atmospheric Sciences*, 70, 2778-2793, 2013.

696 Roesner, S., Flossmann, A., and Pruppacher, H.: The effect on the evolution of the drop
697 spectrum in clouds of the preconditioning of air by successive convective elements,
698 *Quarterly Journal of the Royal Meteorological Society*, 116, 1389-1403, 1990.

699 Rosenfeld, D.: TRMM observed first direct evidence of smoke from forest fires inhibiting
700 rainfall, *Geophysical Research Letters*, 26, 3105-3108, 10.1029/1999gl006066, 1999.

701 Rosenfeld, D.: Suppression of rain and snow by urban and industrial air pollution, *Science*,
702 287, 1793-1796, 10.1126/science.287.5459.1793, 2000.

703 Rosenfeld, D., Lohmann, U., Raga, G. B., O'Dowd, C. D., Kulmala, M., Fuzzi, S., Reissell,
704 A., and Andreae, M. O.: Flood or drought: How do aerosols affect precipitation?,
705 *Science*, 321, 1309-1313, 10.1126/science.1160606, 2008.

706 Saleeby, S. M., Herbener, S. R., van den Heever, S. C., and L'Ecuyer, T.: Impacts of Cloud
707 Droplet–Nucleating Aerosols on Shallow Tropical Convection, *Journal of the*
708 *Atmospheric Sciences*, 72, 1369-1385, 2015.

709 Savane, O. S., Vant-Hull, B., Mahani, S., and Khanbilvardi, R.: Effects of Aerosol on Cloud
710 Liquid Water Path: Statistical Method a Potential Source for Divergence in Past
711 Observation Based Correlative Studies, *Atmosphere*, 6, 273-298, 2015.

712 Seifert, A., and Heus, T.: Large-eddy simulation of organized precipitating trade wind
713 cumulus clouds, *Atmos. Chem. Phys*, 13, 5631-5645, 2013.

714 Seifert, A., Heus, T., Pincus, R., and Stevens, B.: Large-eddy simulation of the transient and
715 near-equilibrium behavior of precipitating shallow convection, *Journal of Advances*
716 *in Modeling Earth Systems*, 2015.

717 Seigel, R. B.: Shallow Cumulus Mixing and Subcloud Layer Responses to Variations in
718 Aerosol Loading, *Journal of the Atmospheric Sciences*, 2014.

719 Seiki, T., and Nakajima, T.: Aerosol effects of the condensation process on a convective
720 cloud simulation, *Journal of the Atmospheric Sciences*, 71, 833-853, 2014.

721 Siebesma, A. P., Bretherton, C. S., Brown, A., Chlond, A., Cuxart, J., Duynkerke, P. G.,
722 Jiang, H., Khairoutdinov, M., Lewellen, D., and Moeng, C. H.: A large eddy
723 simulation intercomparison study of shallow cumulus convection, *Journal of the*
724 *Atmospheric Sciences*, 60, 1201-1219, 2003.

725 Small, J. D., Chuang, P. Y., Feingold, G., and Jiang, H.: Can aerosol decrease cloud lifetime?,
726 *Geophysical Research Letters*, 36, 2009.

727 Squires, P.: The microstructure and colloidal stability of warm clouds, *Tellus*, 10, 262-271,
728 1958.

729 Squires, P., and Twomey, S.: The relation between cloud droplet spectra and the spectrum of
730 cloud nuclei, *Geophysical Monograph Series*, 5, 211-219, 1960.

731 Starr Malkus, J.: Some results of a trade-cumulus cloud investigation, *Journal of*
732 *Meteorology*, 11, 220-237, 1954.

733 Stevens, B.: On the growth of layers of nonprecipitating cumulus convection, *Journal of the*
734 *atmospheric sciences*, 64, 2916-2931, 2007.

735 Stevens, B., and Seifert, R.: Understanding macrophysical outcomes of microphysical choices
736 in simulations of shallow cumulus convection, *Journal of the Meteorological Society*
737 of Japan, 86, 143-162, 2008.

738 Stevens, B., and Feingold, G.: Untangling aerosol effects on clouds and precipitation in a
739 buffered system, *Nature*, 461, 607-613, 10.1038/nature08281, 2009.

740 Takemi, T., Hirayama, O., and Liu, C.: Factors responsible for the vertical development of
741 tropical oceanic cumulus convection, *Geophysical research letters*, 31, 2004.

742 Tao, W.-K., Chen, J.-P., Li, Z., Wang, C., and Zhang, C.: Impact of aerosols on convective
743 clouds and precipitation, *Reviews of Geophysics*, 50, RG2001, 2012.

744 Trenberth, K. E., Fasullo, J. T., and Kiehl, J.: Earth's global energy budget, *Bull. Amer.*
745 *Meteor. Soc.*, 90, 311-323, 2009.

746 Waite, M. L., and Khouider, B.: The deepening of tropical convection by congestus
747 preconditioning, *Journal of the Atmospheric Sciences*, 67, 2601-2615, 2010.

748 Warner, J., and Twomey, S.: The production of cloud nuclei by cane fires and the effect on
749 cloud droplet concentration, *Journal of the atmospheric Sciences*, 24, 704-706, 1967.

750 Xue, H. W., and Feingold, G.: Large-eddy simulations of trade wind cumuli: Investigation of
751 aerosol indirect effects, *Journal of the Atmospheric Sciences*, 63, 1605-1622,
752 10.1175/jas3706.1, 2006.

753 Xue, H. W., Feingold, G., and Stevens, B.: Aerosol effects on clouds, precipitation, and the
754 organization of shallow cumulus convection, *Journal of the Atmospheric Sciences*,
755 65, 392-406, 10.1175/2007jas2428.1, 2008.

756 Yin, Y., K. S. Carslaw, and G. Feingold.: Vertical transport and processing of aerosols in a
757 mixed-phase convective cloud and the feedback on cloud development. *Quarterly*
758 *Journal of the Royal Meteorological Society* 131.605 221-245, 2005.

759 Yuan, T., Remer, L. A., and Yu, H.: Microphysical, macrophysical and radiative signatures of
760 volcanic aerosols in trade wind cumulus observed by the A-Train, *Atmospheric*
761 *Chemistry and Physics*, 11, 7119-7132, 10.5194/acp-11-7119-2011, 2011.

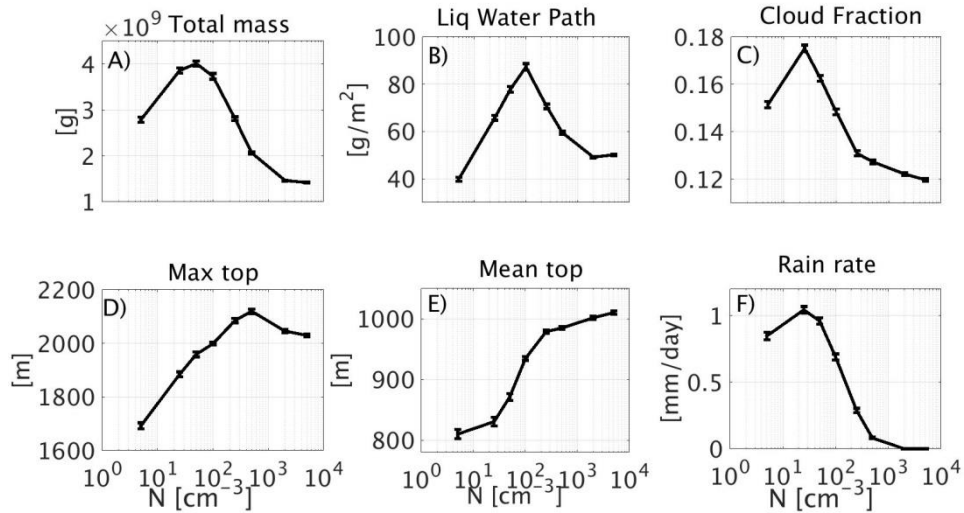
762 Zhao, M., and Austin, P. H.: Life cycle of numerically simulated shallow cumulus clouds.
763 Part I: Transport, *Journal of the Atmospheric Sciences*, 62, 1269-1290,
764 10.1175/jas3414.1, 2005.

765 Zuidema, P., Li, Z., Hill, R. J., Bariteau, L., Rilling, B., Fairall, C., Brewer, W. A., Albrecht,
766 B., and Hare, J.: On trade wind cumulus cold pools, *Journal of the Atmospheric*
767 *Sciences*, 69, 258-280, 2012.

768

769

770



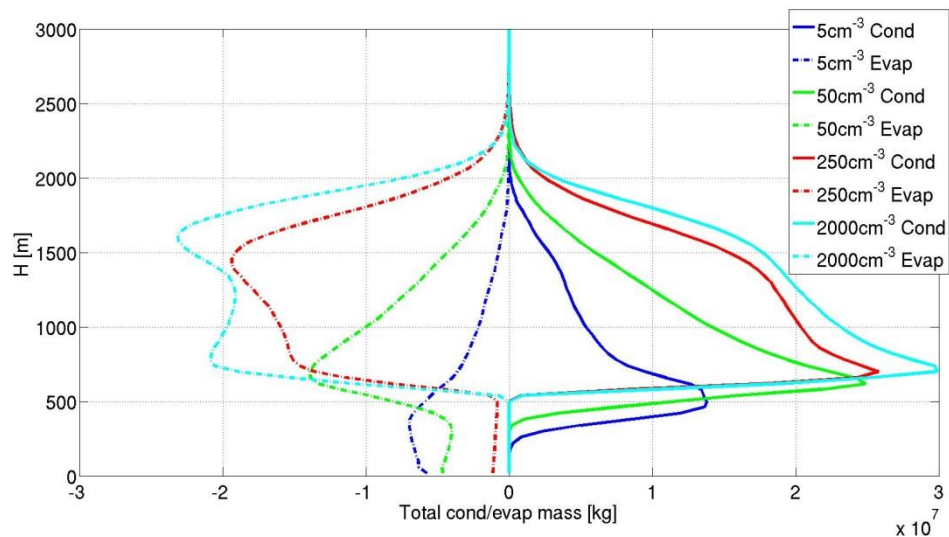
771

772 **Figure 1. mean properties (over domain and time) of the simulated cloud fields as a function of**
 773 **the aerosol concentration used in the simulation: A) total liquid water mass in the domain, B)**
 774 **cloudy LWP, C) cloud fraction (CF) for columns with $\tau > 0.3$, D) maximum cloud top, E) mean**
 775 **cloud top, and, F) surface rain rate. Each of these mean properties are calculated for the last 14**
 776 **hours out of the 16 hours of simulation. The error bars present the standard errors. For details**
 777 **about the different properties see the text.**

778

779

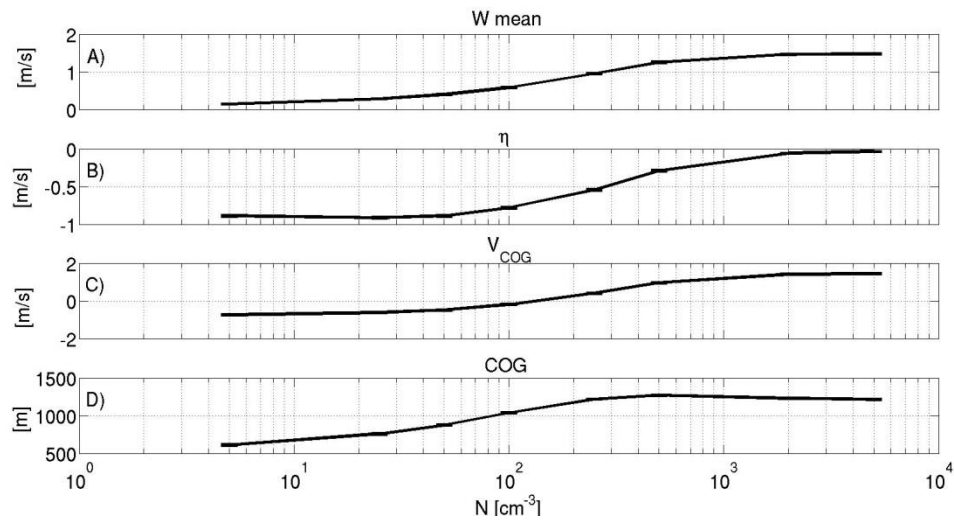
780



781

782 **Figure 2. Domain's total condensed (solid lines) and evaporated mass (dashed lines) for 14 hours**
 783 **of simulation along four different simulations conducted with different aerosol concentration**
 784 **levels (5 cm^{-3} blue, 50 cm^{-3} green, 250 cm^{-3} red and 2000 cm^{-3} cyan).**

785

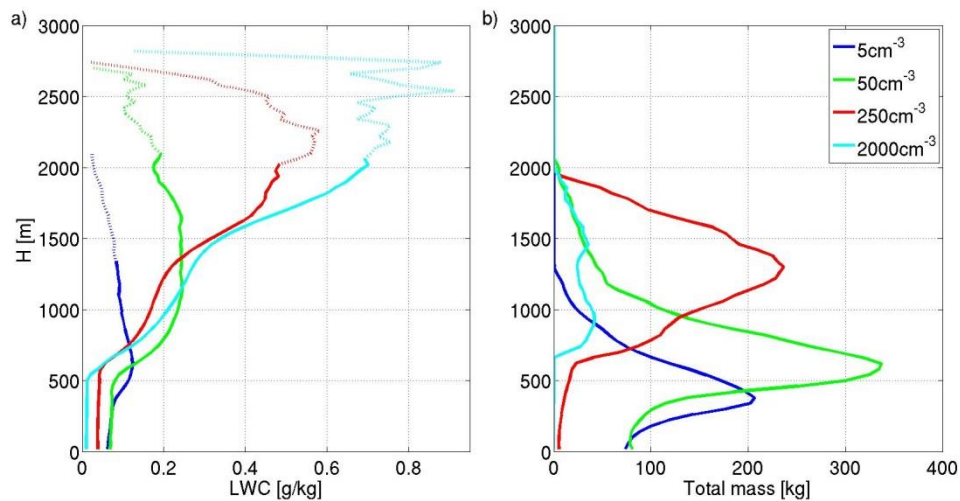


786

787 **Figure 3. Mean (over time and space) of A) updraft (W), B) effective terminal velocity (η), C) the**
788 **center of gravity velocity V_{COG} and D) COG (center of gravity) height as a function of the aerosol**
789 **concentration. All calculated for the last 14 hours out of the 16 hours of simulation.**

790

791

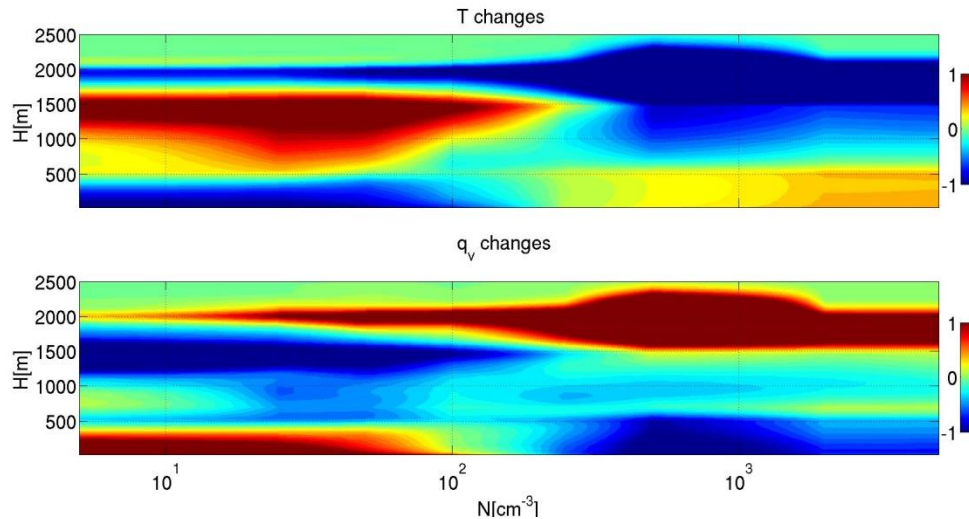


792

793

794 **Figure 4. a) Mean liquid water content (LWC) vertical profiles. b) Vertical profiles of the mean**
795 **(over time) total liquid water mass per height for four different simulations (5 cm^{-3} blue, 50 cm^{-3}**
796 **green, 250 cm^{-3} red and 2000 cm^{-3} cyan). The mean profiles are calculated for the last 14 hours**
797 **out of the 16 hours of simulation. Note that dotted parts of the curves in a) represents heights in**
798 **which the total liquid water mass was less then 1% of the maximum total mass (Fig. 4b).**

799



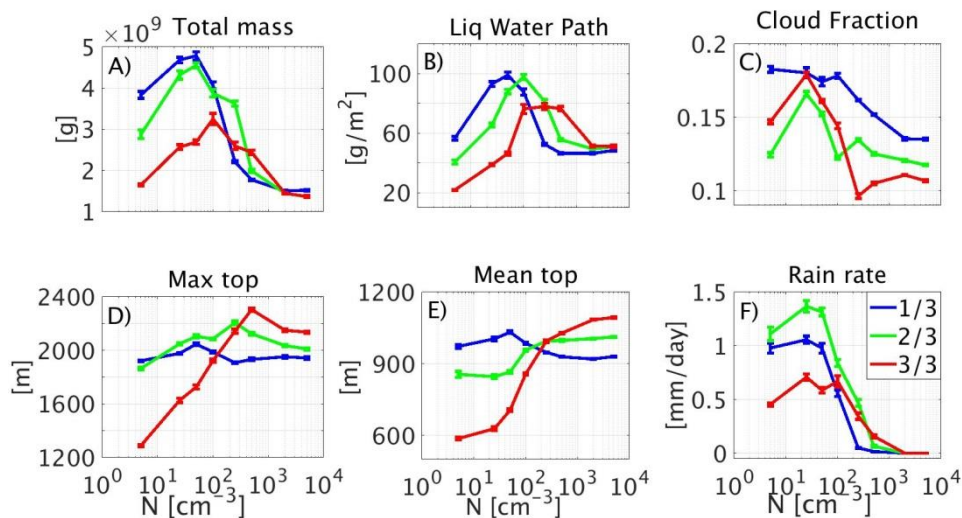
800

801 **Figure 5. Total change, during 16 h of simulation in the temperature ([k] upper panel) and water**
 802 **vapor content ([g/kg] – lower panel) domain mean vertical profiles as a function of the aerosol**
 803 **concentration used in the simulation.**

804

805

806



807

808 **Figure 6. Mean properties (over time and domain) of the simulated cloud fields as a function of**
 809 **the aerosol concentration used in the simulation: A) total liquid water mass in the domain, B)**
 810 **cloudy LWP, C) cloud fraction (CF) for columns with $\tau > 0.3$, D) maximum cloud top, E) mean**
 811 **cloud top, and, F) surface rain rate. Each property is calculated separately for each period of one**
 812 **third of the simulations (blue, green and red for the first, second and third periods, respectively).**
 813 **The error bars present the standard error. For details about the different properties, see the**
 814 **text.**

815

816 **Table 1. change (in %) in key variables between the mean values in the last third period of the**
 817 **simulations and the first period. Negative values are presented in red.**

	Total mass [%]	LWP [%]	COG [%]	Max top [%]	Mean top [%]	W max [%]	CF [%]	Rain rate [%]
5 cm ⁻³	-57.0	-61.4	-43.1	-32.9	-39.7	-28.2	-19.7	-53.5
25 cm ⁻³	-45.2	-58.3	-39.6	-17.8	-37.4	-38.8	-0.6	-32.9
50 cm ⁻³	-43.8	-53.1	-33.7	-15.6	-31.6	-47.9	-7.5	-40.1
100 cm ⁻³	-20.1	-13.0	-16.1	-3.2	-13.0	-32.8	-19.0	19.6
250 cm ⁻³	17.5	48.6	5.0	12.4	5.0	-4.3	-40.7	598.1
500 cm ⁻³	37.4	64.2	19.9	19.2	10.7	9.4	-30.9	841.5
2000 cm ⁻³	-3.7	10.6	14.8	10.1	17.9	6.0	-17.8	-
5000 cm ⁻³	-10.1	5.7	13.7	9.9	17.5	2.9	-20.7	-

818